

---

# HAIR: HYPERNETWORKS-BASED ALL-IN-ONE IMAGE RESTORATION

---

**Jin Cao**

Xi'an Jiaotong University  
2213315515@stu.xjtu.edu.cn

**Yi Cao**

Beijing Computational Science Research Center  
caoyi@csrc.ac.cn

**Li Pang**

Xi'an Jiaotong University  
2195112306@stu.xjtu.edu.cn

**Deyu Meng**

Xi'an Jiaotong University  
dymeng@mail.xjtu.edu.cn

**Xiangyong Cao\***

Xi'an Jiaotong University  
caoxiangyong@mail.xjtu.edu.cn

August 29, 2024

## ABSTRACT

Image restoration aims to recover a high-quality clean image from its degraded version. Recent progress in image restoration has demonstrated the effectiveness of All-in-One image restoration models in addressing various degradations simultaneously. However, these existing methods typically utilize the same parameters to tackle images with different degradation types, thus forcing the model to balance the performance between different tasks and limiting its performance on each task. To alleviate this issue, we propose HAIR, a **Hypernetworks-based All-in-One Image Restoration** method that dynamically generates parameters based on input images. Specifically, HAIR consists of two main components, i.e., Classifier and Hyper Selecting Net (HSN). The Classifier is a simple image classification network used to generate a Global Information Vector (GIV) that contains the degradation information of the input image, and the HSN is a simple fully-connected neural network that receives the GIV and outputs parameters for the corresponding modules. Extensive experiments demonstrate that HAIR can significantly improve the performance of existing image restoration models in a plug-and-play manner, both in single-task and all-in-one settings. Notably, our innovative model, Res-HAIR, which integrates HAIR into the well-known Restormer, can obtain superior or comparable performance compared with current state-of-the-art methods. Moreover, we theoretically demonstrate that our proposed HAIR requires fewer parameters in contrast to the prevalent All-in-One methodologies. The code is available at <https://github.com/toummHus/HAIR>.

## 1 Introduction

Image restoration stands as a pivotal challenge within the field of computer vision, dedicated to the reconstruction of high-quality images from their degraded states. The presence of adverse conditions such as noise, haze, or rain can severely diminish the effectiveness of images for a variety of applications, such as autonomous navigation [1, 2], augmented reality [3, 4, 5]. Therefore, developing robust image restoration methods is of great importance. The use of deep learning in this domain has made remarkable progress, as evidenced by a suite of recent methodologies [6, 7, 8, 9, 10, 11, 12, 13, 14, 15]. Nonetheless, the predominant approach in current research is to employ task-specific models, each tailored to address a particular type of degradation [16, 7, 12, 13, 8]. This tailored approach, while precise, presents a constraint in terms of universality, as it restricts the applicability of models to scenarios with varied or unknown degradations [17, 18, 19]. To overcome this limitation, the research community has increasingly turned its attention to the development of All-in-One image restoration models. These models are designed to tackle various degradations using one single model. Pioneering efforts in this area [20, 21, 1, 22, 23, 24, 25, 26, 15] have utilized a variety of advanced techniques such as contrastive learning [20], meta-learning [25], visual prompting methods

---

\*Corresponding Author

[24, 27, 28, 14]. These approaches have undoubtedly made substantial contributions to the field, propelling it forward with notable advancements.

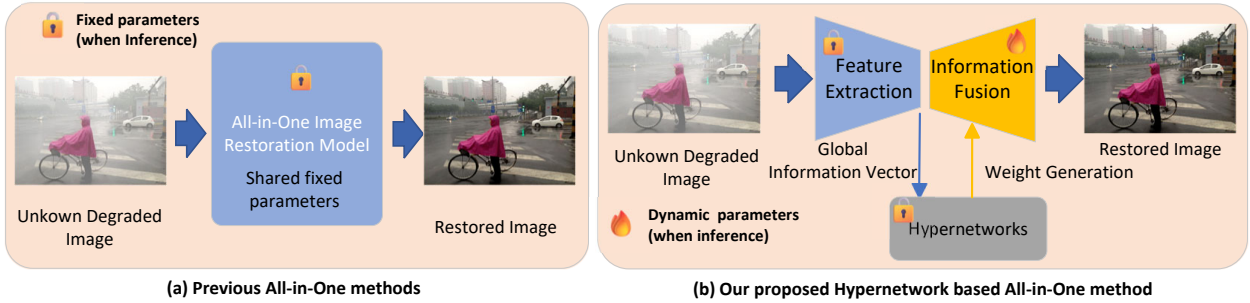


Figure 1: The difference between our method and previous methods. (a) Previous All-in-One image restoration methods. For images with various degradations, these methods utilize a single model with the same parameters. (b) Our proposed HAIR. Given a certain degraded image, we first use a fixed Extraction module to extract the features, and feed the extracted feature into the Hypernetwork to generate the dynamic parameters for the fusion module and finally get the restored image by the generated parameters.

Despite the notable successes of these methods, they share a common drawback, namely, they rely on a single model with fixed parameters to address a variety of degradations. This one-size-fits-all approach can hinder the model’s effectiveness when dealing with multiple degradations simultaneously. For example, when viewed through the lens of frequency domain analysis, haze is characterized as low-frequency noise, in contrast to rain, which is considered high-frequency interference. An effective dehazing model acts as a low-pass filter, preserving high-frequency details, whereas deraining requires the opposite—enhancing the high-frequency components. Consequently, a model must strike a balance between these conflicting demands of different degradations, which may lead to suboptimal performance.

To mitigate the aforementioned issue, we propose HAIR in this paper. Our fundamental concept is the dynamic generation of parameters (weights) based on the degradation information present in the input image. HAIR employs Hypernetworks [29], a trainable neural network that outputs parameters for other neural networks, to take the degradation information from the input image and produce corresponding parameters. Specifically, for a given unknown degraded image, we first utilize a Classifier, similar to those used in image classification networks, to obtain its Global Information Vector, which contains crucial discriminative information about various types of image degradation (as shown in Fig. 2). This vector is then passed to the Hyper Selecting Net, which is a Fully Connected Network, to generate the requisite parameters, as illustrated in Fig. 1. Therefore, our method can dynamically adapt to various degradations. With these dynamically parameterised modules, we ultimately achieve the restored image. In brief, our contributions include:

- We propose HAIR, a novel Hypernet-based All-in-One image restoration method capable of dynamically generating parameters based on the input image’s characteristics. HAIR consists of two components, i.e. Classifier and Hyper Selecting Nets, both of which function as a plug-in-and-play module. Extensive experiments demonstrate that HAIR can significantly improve the performance of existing image restoration models in a plug-and-play manner, both in single-task and all-in-one settings.
- By incorporating HAIR into Restormer [12], we propose a new all-in-one model, i.e. Res-HAIR. To the best of our knowledge, our method is the first to apply data-adaptive Hypernetworks to All-in-One image restoration models. Extensive experiments validate that the proposed Res-HAIR can achieve superior or comparable performance compared with current state-of-the-art methods across a variety of image restoration tasks.
- We theoretically prove that, for a given small error threshold  $\epsilon$  in image restoration tasks, HAIR requires fewer parameters compared to mainstream embedding based All-in-One methods like [20, 24, 26].

## 2 Related Preliminaries

### 2.1 All-in-One Image Restoration

While single degradation methods do achieve great success [9, 10, 11, 7, 12, 13], blind all-in-one image restoration, which aims to utilize a single deep blind restoration model to tackle multiple types of degradation simultaneously without the prior information of the degradation of the input image, has gained more attention recently [1, 2, 30, 24, 25, 26]. The seminal work AirNet [20] achieves blind All-in-One image restoration by employing contrastive learning to extract degradation representations from corrupted images, which are subsequently utilized to restore the clean image.

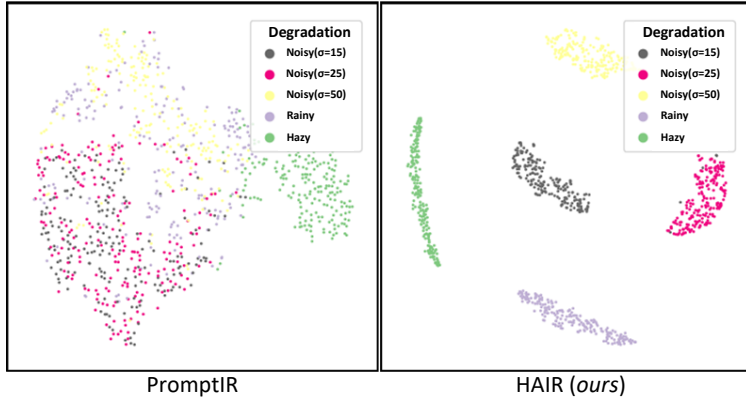


Figure 2: The figure presents tSNE plots of the degradation embeddings utilized in PromptIR [24] and our HAIR. Each distinct color represents a unique degradation type. It becomes evident that HAIR excels not only in recognizing various degradation types, such as noise, rain, and haze, but also in distinguishing between the same type of degradation at varying intensities, exemplified by noise with standard deviations of [15, 25, 50]. This capability underscores HAIR’s remarkable adaptability and generalization when confronted with diverse degradation scenarios.

Next, IDR [25] decomposes image degradations into their underlying physical principles, achieving All-in-One image restoration through a two-stage process based on meta-learning. With the rise of LLM [31], prompt-based learning [24, 27, 14] has also emerged as a promising direction in computer vision tasks. Despite the success these methods have achieved, they typically use the same parameters for distinct degradations and inject the degradation information as conditional embeddings into the model, which may impair the performance of the models. In contrast, our proposed HAIR can adaptively generate specific parameters for the given degraded image, resulting in better generalization to unknown degradations. [32] theoretically explains why using data-conditional Hypernetworks to generate adaptive parameters works better than injecting conditional embeddings into the model.

## 2.2 Image Classification and Feature Extraction

Image classification is a fundamental task in Computer Vision, with the goal of categorizing images based on their content [33]. Typically, image classification contains two key steps: feature extraction and classification. The primary challenge in this task is feature extraction, which involves converting an image into a vector that encapsulates its most critical information. While traditional methods relied on handcrafted techniques [34], the advent of neural networks has revolutionized feature extraction [35, 36, 37, 38]. Given that these vectors are capable of classifying hundreds of categories [39], they must contain the essential information of the images. This concept also extends to the classification of degraded images. For instance, if we categorize degraded images into different types, e.g. noisy, rainy, or hazy, and by levels of degradation like slightly noisy, moderately noisy, and very noisy, the feature vectors should be effective in classifying these variations. The rationale is that recognizing different degradations is generally less complex than identifying hundreds of distinct objects. Therefore, our proposed method employs a Classifier to obtain a Global Information Vector (GIV), that captures the rich global information of the image, including its degradation characteristics. (As shown in Fig. 2) This GIV is then utilized to generate parameters tailored to the specific degradation present in the image.

## 2.3 Data-conditioned Hypernetworks

Hypernetworks [29] are a class of neural networks designed to generate weight values (parameters) for other networks. They can be broadly classified into three main types: Task-conditioned, Data-conditioned, and Noise-conditioned hypernetworks [40]. Among these methods, Data-conditioned hypernetworks are particularly noteworthy for their ability to generate weights contingent upon the distinctive features of the input data. This capability allows the neural network to dynamically adapt its behaviour in response to specific input patterns or characteristics, fostering flexibility and adaptability within the model. Consequently, this results in enhanced generalization and robustness. Data-conditioned Hypernetworks have found applications across the field of computer vision, including semantic segmentation [41] and image editing [42]. Despite previous attempts to integrate Hypernetworks into Image Restoration [43], these have primarily leveraged Task-conditioned hypernetworks. Such an approach cannot fully harness the potential of hypernetworks for the task of image restoration. To the best of our knowledge, our work first introduces Data-conditioned hypernetworks to the domain of image restoration, unlocking new possibilities for the field.

## 3 Method

In this section, we outline the core principles of our proposed effective all-in-one image restoration method. Note that we use **Res-HAIR** stands for **Restormer embedded with HAIR**.

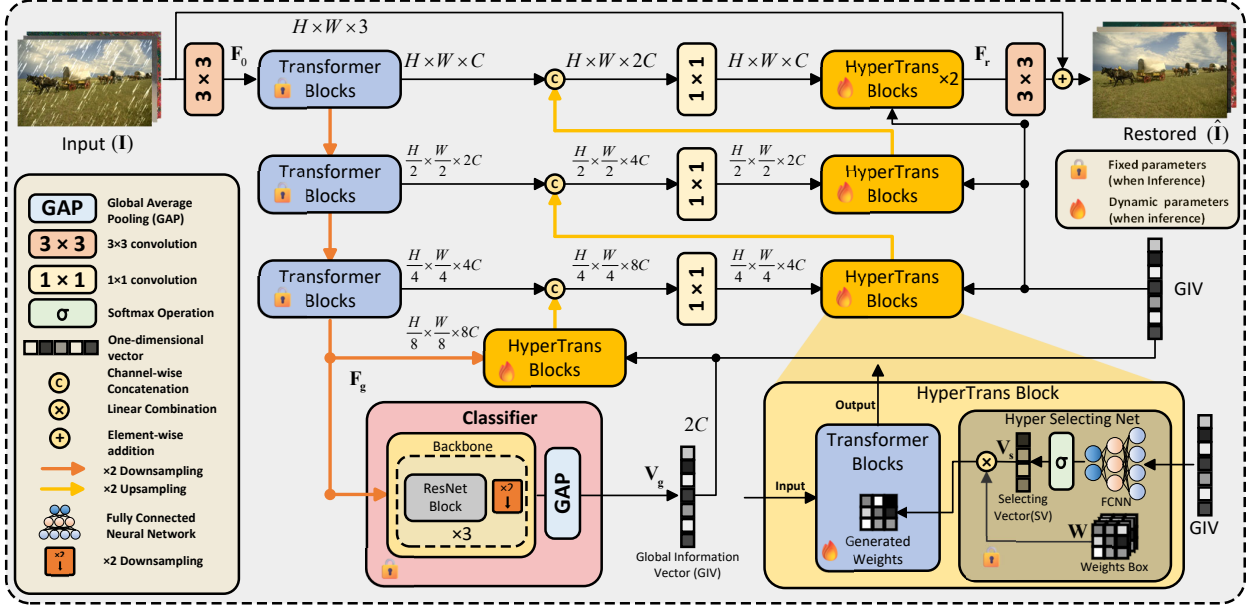


Figure 3: The overall framework of Res-HAIR. In this paper, we mainly incorporate HAIR into Restormer [12], which has demonstrated robust performance in all-in-one restoration scenarios [24, 26, 28]. HAIR introduces a Classifier that yields a Global Information Vector (GIV)  $\mathbf{V}_g$  from the high-level feature  $\mathbf{F}_g$  encapsulating the input image’s degradation information. Additionally, the Hyper Selecting Nets (HSNs) dynamically generate weights for the Transformer Blocks based on GIV, customizing the restoration process to address the specific degradation characteristics of each image. This innovative approach allows models to adapt to various image restoration tasks without altering the original architecture. **For other baseline models, we follow a similar integration approach with HAIR: we introduce a classifier at the network’s midpoint and utilize the resulting GIV to dynamically generate weights for the subsequent layers of the network.**

**Overall Pipeline** As shown in Fig. 3, our network architecture is consistent with Restormer [12]. Given a certain degraded image input  $\mathbf{X} \in \mathbb{R}^{H \times W \times 3}$ , Res-HAIR utilizes a  $3 \times 3$  convolution to transform  $\mathbf{X}$  into feature embeddings  $\mathbf{F}_0 \in \mathbb{R}^{H \times W \times C}$ , where  $C$  denotes the number of channels. These feature embeddings are then proceeded through a 4-level hierarchical encoder-decoder, resulting in deep features  $\mathbf{F}_r$ . Each level of the encoder-decoder incorporates several Transformer blocks, with an increasing number from the top to the bottom level, ensuring computational efficiency. The left three blue "Transformer Blocks" function as an Encoder, designed to extract features from  $\mathbf{F}_0$  and ultimately produce a global feature map  $\mathbf{F}_g \in \mathbb{R}^{\frac{H}{8} \times \frac{W}{8} \times 8C}$  with a large receptive field.  $\mathbf{F}_g$  is then input into a Classifier to yield a Global Information Vector (GIV)  $\mathbf{V}_g \in \mathbb{R}^{2C}$ . The right four orange "HyperTrans Blocks" operate as a Decoder, aiming to adaptively fuse features at each Decoder level based on degradation, culminating in a restored image  $\hat{\mathbf{X}}$ . Specifically, at each Decoder level, the HyperTrans Block accepts two inputs: the input feature and the GIV  $\mathbf{V}_g$ .  $\mathbf{V}_g$  is fed into the Hyper Selecting Net to generate weights for the corresponding Transformer Blocks, which are then applied to the input feature to produce the output. It is important to note that all HyperTrans Blocks use **the same**  $\mathbf{V}_g$  derived from  $\mathbf{F}_g$ . Since the weights in the Decoder are generated based on  $\mathbf{V}_g$ , which contains the degradation information of  $\mathbf{X}$ , our method exhibits strong generalization and adaptability, leading to excellent restoration performance.

### 3.1 Classifier

As outlined in Section 2.2, our approach to extracting degradation information involves designing a straightforward Classifier akin to those used in image classification tasks. We start by entering  $\mathbf{F}_g \in \mathbb{R}^{\frac{H}{8} \times \frac{W}{8} \times 8C}$  into the backbone, which is composed of multiple ResNet blocks [35] followed by downsampling  $\times 2$ . This process is aimed at downsizing the spatial resolution while distilling the essential information, as depicted by the following equations:

$$\begin{aligned} \mathbf{F}_g^1 &= \text{Downsampling}(\text{ResNetBlock}(\mathbf{F}_g)), \\ \mathbf{F}_g^t &= \text{Downsampling}(\text{ResNetBlock}(\mathbf{F}_g^{t-1})), \quad \text{for } t = 1, 2, 3. \end{aligned} \quad (1)$$

After three iterations, we obtain  $\mathbf{F}_g^3 \in \mathbb{R}^{\frac{H}{64} \times \frac{W}{64} \times 2C}$ , which serves as the input for generating the GIV  $\mathbf{V}_g \in \mathbb{R}^{2C}$ :

$$\mathbf{V}_g = \text{GAP}(\mathbf{F}_g^3), \quad (2)$$

where GAP denotes Global Average Pooling. The inclusion of GAP ensures that  $\mathbf{V}_g$  remains a one-dimensional vector of consistent size, irrespective of the input image’s resolution. Unlike traditional image classification networks, there is no requirement for a Softmax layer here, as its application would confine the values of  $\mathbf{V}_g$  within the  $[0,1]$  range, potentially restricting the parameter generation process. Moreover, the backbone can be substituted with other straightforward image classification networks such as VGG [44] and Inception [45], without any detrimental impact on performance, given that the classification of degradation types is a relatively simple task.

### 3.2 Hyper Selecting Net

Upon obtaining the Global Information Vector  $\mathbf{V}_g$  from the Classifier, it is fed into our Data-conditioned Hypernetworks, known as Hyper Selecting Nets, to generate weights for the corresponding Transformer Blocks. Given  $\mathbf{V}_g \in \mathbb{R}^{2C}$ , a Selecting Vector (SV)  $\mathbf{V}_s \in \mathbb{R}^N$  is initially computed as follows:

$$\mathbf{V}_s = \sigma(\text{FCNN}(\mathbf{V}_g)). \quad (3)$$

Here,  $\sigma$  stands for a Softmax operation and FCNN denotes a simple Fully-Connected Neural Network. Subsequently, the parameters  $\mathbf{w}$  are derived as

$$\mathbf{w} = \sum_{i=1}^N \mathbf{V}_s^i \mathbf{W}_i. \quad (4)$$

In this formula,  $\mathbf{V}_s^i$  represents the  $i$ -th element of  $\mathbf{V}_s$ . The matrix  $\mathbf{W} \in \mathbb{R}^{N \times P}$ , referred to as the Weights Box, comprises  $\mathbf{W}_i \in \mathbb{R}^P$  as its  $i$ -th column. The hyperparameter  $N$  influences the total number of parameters, with  $P$  being the count of parameters required for one Transformer Block. With  $\mathbf{w}$  determined, it is then applied as parameters for the Transformer Block:

$$\mathbf{x}' = \text{Transformer\_Block}(\mathbf{x}; \mathbf{w}). \quad (5)$$

Here,  $\mathbf{x}$  signifies the input, and  $\mathbf{x}'$  is the resulting output. As the Transformer Blocks [12] are based on convolution,  $\mathbf{w} \in \mathbb{R}^P$  is reshaped into 4-dimensional tensors to serve as convolution kernels for the Transformer Blocks. To economize on parameters, Transformer Blocks at the same decoder level share one Weights Box, and each Transformer Block is independently equipped with its own FCNN.

### 3.3 Rethinking Weights Generation via a Selecting Perspective

If we consider the Weights Box as part of the FCNN, it may not be immediately clear why such a direct derivation of weights from a neural network works well. This seeming lack of intuitiveness is what we aim to address. Before delving into the explanation, we establish a foundational proposition:

**Proposition 1. (Convolution operations exhibit the distributive law over addition)** Let  $\mathbf{x} \in \mathbb{R}^{H \times W \times C}$  be the input feature, and let  $w_i, i = 1, 2, \dots, n$  represent the convolution kernels. The law is mathematically expressed as:

$$\mathbf{x} * \left( \sum_{i=1}^n w_i \right) = \sum_{i=1}^n (\mathbf{x} * w_i) \quad (6)$$

where  $*$  denotes the standard 2-dimensional convolution.

With this proposition, the following formula becomes evident:

$$\mathbf{x} * \mathbf{w} = \mathbf{x} * \left( \sum_{i=1}^N \mathbf{V}_s^i \mathbf{W}_i \right) = \sum_{i=1}^N (\mathbf{x} * (\mathbf{V}_s^i \mathbf{W}_i)) = \sum_{i=1}^N \mathbf{V}_s^i (\mathbf{x} * \mathbf{W}_i), \quad (7)$$

where the constraint  $\sum_{i=1}^N \mathbf{V}_s^i = 1$  holds due to the property of Softmax operation. In essence, the convolution with the generated weights is equivalent to a weighted sum of convolutions between the input  $\mathbf{x}$  and each kernel  $\mathbf{W}_i$  in the Weights Box. This process can be seen as a process of **selecting convolution kernels**. For instance, with a Weights Box  $\mathbf{W} \in \mathbb{R}^{2 \times P}$  that includes a low-pass  $\mathbf{W}_1$  and a high-pass  $\mathbf{W}_2$ , the rainy input  $\mathbf{x}_1$  would ideally have a larger  $\mathbf{V}_s^1$  to filter out high-frequency noise, while a smaller  $\mathbf{V}_s^2$  would help retain details. Conversely, for a hazy input  $\mathbf{x}_2$ , a larger  $\mathbf{V}_s^2$  would be necessary to mitigate low-frequency haze. Although real-world degradations can be more complex, our Hyper Selecting Net can adaptively select the appropriate weights. This insight into the selection process helps us understand HAIR, namely, for each input, the Hyper Selecting Net produces a tailored Selecting Vector and adaptively chooses the most suitable convolution kernel. Given that core operations such as convolution and matrix multiplication follow the distributive law over addition, HAIR is versatile and can be integrated into various architectures like Transformer [46] and Mamba [47].

### 3.4 A Brief Analysis of Model Complexity

In Section 2.3, we claim that our Hypernetworks-based method can work better than conditional embedding-based methods like AirNet [20] and PromptIR [24]. This section will give a simple proof for this point. In the context of all-in-one image restoration, we aim to find a function  $f : \mathbb{R}^{3HW} \rightarrow \mathbb{R}^{3HW}$  to map a degraded image  $\mathbf{X}$  to a restored image  $\hat{\mathbf{X}}$  by minimizing the distance between  $\hat{\mathbf{X}}$  and the ground truth  $\mathbf{Y} = y(\mathbf{X})$ .<sup>2</sup> Mainstream methods typically utilize a neural network  $g(\mathbf{X}, e(\mathbf{X}))$  to learn the mapping, where  $e(\mathbf{X}) \in \mathbb{R}^k$  stands for the degradation information (degradation embedding) from the input image, such as the prompt in PromptIR [24]. These methods directly send  $e(\mathbf{X})$  together with  $\mathbf{X}$  into the network to get  $\hat{\mathbf{X}}$ . For our HAIR, the neural network can be formulated as  $h(\mathbf{X}; \theta(e(\mathbf{X})))$ , where  $\theta$  is a function that maps  $e(\mathbf{X})$  into the parameters of  $h$ . We define the distance between the two functions as:

$$d(g, y) = \min_g \max_{\mathbf{X}} \|g(\mathbf{X}, e(\mathbf{X})) - y(\mathbf{X})\|_{\infty}. \quad (8)$$

Given that vector functions can be complex, we define a scalar function  $f^i : \mathbb{R}^M \rightarrow \mathbb{R}, i = 1, 2, 3 \dots M$ . of a vector function  $f : \mathbb{R}^M \rightarrow \mathbb{R}^M$ .  $f^i$  means  $f^i$  produce the  $i$ -th value of  $f$ , then we have:

$$\begin{aligned} d(g, y) &= \min_g \max_{\mathbf{X}} \max_i |g^i(\mathbf{X}) - y^i(\mathbf{X})| \\ &= \min_g \max_i \max_{\mathbf{X}} |g^i(\mathbf{X}) - y^i(\mathbf{X})| \\ &= \min_g \max_{\mathbf{X}} |g^{k(g)}(\mathbf{X}) - y^{k(g)}(\mathbf{X})|. \end{aligned} \quad (9)$$

Since the value range of  $i$  is limited, given the function  $g$ , we can always find an integer  $k(g)$  to replace  $\max_i$ . To complete the proof, we need some assumptions.

**Assumption 1.** *The target function  $y^i \in \mathcal{W}_{r,3HW}, i = 1, 2, \dots, 3HW$ . The Sobolev space  $\mathcal{W}_{r,3HW}$  is the set of functions that are  $r$ -times differentiable with all  $r$ -th order derivatives being continuous and bounded by the Sobolev norm  $\leq 1$ , defined on  $\mathbb{R}^{3HW}$ .*

Intuitively, since  $y^i$  maps the degraded image to a single pixel of the clean image, a little disturbance on the degraded image should only bring a little difference to the single pixel, so  $y^i$  should be smooth and differentiable or at least continue. What's more, the domain and range of  $y$  are restricted to  $[0, 1]^{3HW}$ , with most of the pixels far less than 1, the Sobolev norm of  $y_i$  can be generally less than 1. So this assumption generally holds.

**Assumption 2.** *For various functions (especially neural networks)  $g$ , the integer  $k(g)$  in Eq. (9) remains the same.*

In our context, the various  $g$  represents the same network with different weights during training. No matter how the parameters update, the most "difficult" degraded image generally remains the same one, e.g., the one with very severe degradation. Within this "difficult" image, the most "difficult" pixel should also remain the same, e.g., the pixel that varies dramatically from its clean version. In this way, we simplify the vector function  $g$  to scalar function  $g^{k(g)}$ . With these two assumptions, as well as incorporating Theorem 2-4 and all the assumptions in [32], we can obtain the following conclusion.

**Theorem 1.** *For conditional embedding-based all-in-one image restoration methods  $g(\mathbf{X}, e(\mathbf{X}))$  like PromptIR [24], to achieve error  $d(g, y) \leq \epsilon$ , the complexity (number of parameters) of the corresponding model is at least  $N_g = \Omega(\epsilon^{-3HW-k})$ .*

**Theorem 2.** *For Hypernetworks based methods  $h(\mathbf{X}; \theta(e(\mathbf{X})))$  like our HAIR, to achieve error  $d(h, y) \leq \epsilon$ , the complexity of the corresponding model is  $N_{\theta} = O(\epsilon^{-3HW/r})$ .*

Please refer to paper [32] and Section 6.1 for detailed premises and proof of Theorem 1 and 2. The two Theorems demonstrate that to achieve the same error  $\epsilon$ , our proposed HAIR requires fewer parameters than conditional embedding-based methods. (As long as  $\epsilon$  is small enough.)

## 4 Experiments

We conduct experiments by rigorously adhering to the methodologies established in prior research on general image restoration [25, 24], under two distinct experimental configurations: (a) All-in-One and (b) Single-task. In the All-in-One configuration, a singular model is trained to handle multiple types of degradation, encompassing both three and five unique degradations. In contrast, the Single-task configuration involves the training of individual models dedicated to specific restoration tasks.

<sup>2</sup>For the sake of discussion, the following tensors are generally regarded as flattened one-dimensional vectors.

## 4.1 Experimenting Preparation

**Implementation Details.** Our Res-HAIR framework is designed to be end-to-end trainable, eliminating the need for pre-training any of its components. The architecture comprises a 4-level encoder-decoder structure, with each level equipped with a varying number of Transformer blocks. Specifically, the number of blocks increases progressively from level-1 to level-4, following the sequence [4, 6, 6, 8]. HyperTrans Blocks are employed throughout level-4 and the decoding stages of levels 1-3. Additionally, the Weights Box parameter  $N$  is set according to the sequence [5, 7, 7, 9] for each respective level. In the all-in-one setting, the model is trained with a batch size of 32, while in the single-task setting, a batch size of 8 is used. The optimization of the network is guided by an  $L_1$  loss function, employing the AdamW optimizer [48] with parameters  $\beta_1 = 0.9$  and  $\beta_2 = 0.999$ . The learning rate is set to  $2e - 4$  for the initial 150 epochs, and we change it to  $2e - 5$  for the final 10 epochs. To enhance the training data, input patches of size  $128 \times 128$  are utilized, with random horizontal and vertical flips applied to the images to augment the dataset.

**Datasets.** We follow the approaches in previous studies [20, 24, 25] for our All-in-One and single-task experiments, using the following datasets. For single-task image denoising, we use the BSD400 [49] and WED [50] datasets, adding Gaussian noise at levels  $\sigma \in \{15, 25, 50\}$  to generate training images. Testing is performed on the BSD68 [51] and Urban100 [52] datasets. For deraining, we employ the Rain100L dataset [53]. Dehazing experiments utilize the SOTS dataset [54]. Deblurring and low-light enhancement tasks use the GoPro [55] and LOL-v1 [56] datasets respectively. To create a comprehensive model for all tasks, we combine these datasets and train them in a setting that covers three or five types of degradations. For single-task models, training is conducted for the same duration on the respective dataset.

Table 1: *Comparison to state-of-the-art on three degradations.* PSNR (dB,  $\uparrow$ ) and SSIM ( $\uparrow$ ) metrics are reported on the full RGB images. **Best** and **second best** performances are highlighted. Our method sets a new state-of-the-art on average across all benchmarks while being significantly more efficient than previous work. ‘-’ represents unreported results.

Method	Params.	Dehazing		Deraining		Denoising					Average		
		SOTS	Rain100L	BSD68 $_{\sigma=15}$	BSD68 $_{\sigma=25}$	BSD68 $_{\sigma=50}$							
BRDNet [57]	-	23.23	.895	27.42	.895	32.26	.898	29.76	.836	26.34	.693	27.80	.843
LPNet [58]	-	20.84	.828	24.88	.784	26.47	.778	24.77	.748	21.26	.552	23.64	.738
FDGAN [59]	-	24.71	.929	29.89	.933	30.25	.910	28.81	.868	26.43	.776	28.02	.883
DL [23]	2M	26.92	.931	32.62	.931	33.05	.914	30.41	.861	26.90	.740	29.98	.876
MPRNet [21]	16M	25.28	.955	33.57	.954	33.54	.927	30.89	.880	27.56	.779	30.17	.899
Restormer [12]	26M	29.92	.970	35.56	.969	33.86	.933	31.20	.888	27.90	.794	31.68	.910
AirNet [20]	9M	27.94	.962	34.90	.967	33.92	.933	31.26	.888	28.00	.797	31.20	.910
PromptIR [24]	36M	30.58	.974	36.37	.972	<b>33.98</b>	<b>.933</b>	<b>31.31</b>	<b>.888</b>	<b>28.06</b>	<b>.799</b>	32.06	.913
DaAIR[26]	6M	<b>32.30</b>	<b>.981</b>	<b>37.10</b>	<b>.978</b>	33.92	.930	31.26	.884	28.00	.792	<b>32.51</b>	<b>.913</b>
Res-HAIR ( <i>ours</i> )	29M	<b>30.98</b>	<b>.979</b>	<b>38.59</b>	<b>.983</b>	<b>34.16</b>	<b>.935</b>	<b>31.51</b>	<b>.892</b>	<b>28.24</b>	<b>.803</b>	<b>32.70</b>	<b>.919</b>

## 4.2 Results

**All-in-One: Three degradations.** We conducted a comparative evaluation of our All-in-One image restoration framework against several state-of-the-art specialized methods, including BRDNet [57], LPNet [58], FDGAN [59], DL [23], MPRNet [21], AirNet [20], PromptIR [24], and DaAIR [26]. Each of these methods was trained to handle the tasks of dehazing, deraining, and denoising. As illustrated in Table 1, our approach excels as the leading contender, offering a significant average improvement of 0.64 dB over PromptIR [24]. Our method notably outperforms existing benchmarks on BSD68 and Rain100L datasets, setting a new precedent by exceeding the performance of the previous best methods by margins of 0.19 dB and 1.49 dB respectively.

**All-in-One: Five Degradations.** Following recent studies [25, 26], we have extended our approach to include deblurring and low-light image enhancement, thereby broadening our three-degradation framework to a more complex All-in-One setting. As demonstrated in Table 2, our method excels by learning specialized models for each degradation type while effectively capturing the shared characteristics between tasks. It achieves an average improvement of 0.6 dB over PromptIR [24] and 0.13 dB over DaAIR [26], establishing a new benchmark for state-of-the-art (SOTA) performance across all five benchmarks. Additionally, we compared our method with general image restoration models trained in the same All-in-One setting. Notably, our method significantly outperforms our baseline (i.e. Restormer [12]) in various tasks. This comparison highlights the strong capability of our method as a versatile plug-in-and-play module, enhancing the performance of existing restoration architectures with minimal integration complexity.

Table 2: Comparison to state-of-the-art on five degradations. PSNR (dB,  $\uparrow$ ) and SSIM ( $\uparrow$ ) metrics are reported on the full RGB images with (\*) denoting general image restorers, others are specialized all-in-one approaches. **Best** and **second best** performances are highlighted.

Method	Params.	Dehazing		Deraining		Denoising		Deblurring		Low-Light		Average
		SOTS		Rain100L		BSD68 $_{\sigma=25}$		GoPro		LOLv1		
NAFNet* [8]	17M	25.23	.939	35.56	.967	31.02	.883	26.53	.808	20.49	.809	27.76 .881
DGUNet* [60]	17M	24.78	.940	36.62	.971	31.10	.883	27.25	.837	21.87	.823	28.32 .891
SwinIR* [7]	1M	21.50	.891	30.78	.923	30.59	.868	24.52	.773	17.81	.723	25.04 .835
Restormer* [12]	26M	24.09	.927	34.81	.962	31.49	.884	27.22	.829	20.41	.806	27.60 .881
DL [23]	2M	20.54	.826	21.96	.762	23.09	.745	19.86	.672	19.83	.712	21.05 .743
Transweather [1]	38M	21.32	.885	29.43	.905	29.00	.841	25.12	.757	21.21	.792	25.22 .836
TAPE [22]	1M	22.16	.861	29.67	.904	30.18	.855	24.47	.763	18.97	.621	25.09 .801
AirNet [20]	9M	21.04	.884	32.98	.951	30.91	.882	24.35	.781	18.18	.735	25.49 .847
IDR [25]	15M	25.24	.943	35.63	.965	<b>31.60</b>	<b>.887</b>	27.87	.846	21.34	.826	28.34 .893
PromptIR [24]	36M	30.61	.974	36.17	.973	31.25	.887	27.93	.851	<b>22.89</b>	<b>.842</b>	29.77 .905
DaAIR [26]	6M	<b>31.97</b>	<b>.980</b>	<b>36.28</b>	<b>.975</b>	31.07	.878	<b>29.51</b>	<b>.890</b>	22.38	.825	<b>30.24</b> <b>.910</b>
Res-HAIR (ours)	29M	<b>30.62</b>	<b>.978</b>	<b>38.11</b>	<b>.981</b>	<b>31.49</b>	<b>.891</b>	<b>28.52</b>	<b>.874</b>	<b>23.12</b>	<b>.847</b>	<b>30.37</b> <b>.914</b>

**Single-Degradation Results.** To evaluate the effectiveness of our proposed method, we provide results in Table 3, which show the performance of individual instances of our method trained under a single degradation protocol. Specifically, the single-task variant dedicated to deraining consistently achieves higher performance than PromptIR [24] and DaAIR by margins of 1.96 dB and 1.22 dB, respectively. When applied to image denoising, our method also demonstrates superiority over the aforementioned approaches, with an improvement of 0.21 dB and 0.47 dB, respectively. These results underscore the significant enhancements in performance delivered by our method.

Table 3: Comparison to state-of-the-art for single degradations. PSNR (dB,  $\uparrow$ ) and SSIM ( $\uparrow$ ) metrics are reported on the full RGB images. **Best** and **second best** performances are highlighted. Our method excels prior work on deraining and denoising.

(a) Dehazing		(b) Deraining		(c) Denoising			
Method	SOTS	Method	Rain100L	Method	$\sigma=15$	$\sigma=25$	$\sigma=50$
DehazeNet [61]	22.46 .851	DIDMDN [64]	23.79 .773	CBM3D [68]	33.93 .941	31.36 .909	27.93 .833
MSCNN [62]	22.06 .908	UMR [65]	32.39 .921	DnCNN [69]	32.98 .931	30.81 .902	27.59 .833
EPDN [63]	22.57 .863	SIRR [66]	32.37 .926	IRCNN [6]	27.59 .833	31.20 .909	27.70 .840
FDGAN [59]	23.15 .921	MSPFN [67]	33.50 .948	FFDNet [70]	33.83 .942	31.40 .912	28.05 .848
Restormer [12]	30.87 .969	Restormer [12]	36.74 .978	BRDNet [57]	34.42 .946	31.99 .919	28.56 .858
AirNet [20]	23.18 .900	AirNet [20]	34.90 .977	AirNet [20]	34.40 .949	32.10 .924	28.88 .871
PromptIR [24]	31.31 .973	PromptIR [24]	37.04 .979	PromptIR [24]	<b>34.77</b>	<b>.952</b>	<b>32.49</b>
DaAIR [26]	<b>31.99</b> <b>.981</b>	DaAIR [26]	<b>37.78</b> <b>.982</b>	DaAIR [26]	<b>.929</b>	<b>.929</b>	<b>29.39</b> <b>.881</b>
Res-HAIR (ours)	<b>31.68</b> <b>.980</b>	Res-HAIR (ours)	<b>39.00</b> <b>.985</b>	Res-HAIR (ours)	<b>34.93</b>	<b>.953</b>	<b>32.70</b>
					<b>.931</b>	<b>.931</b>	<b>29.65</b> <b>.885</b>

**Visual Results** The visual results captured under three degradation scenarios are presented in Fig. 4. These results clearly demonstrate the superiority of our method in terms of visual quality: In the denoising task at  $\sigma = 25$ , Res-HAIR retains more fine details compared to other methods; in the deraining task, Res-HAIR effectively removes all rain streaks, whereas the compared methods exhibit noticeable remnants; in the dehazing task, Res-HAIR may not closely resemble the Ground Truth, yet it provides the most visually pleasing outcome and even clears the original haze present in the Ground Truth. Collectively, these observations confirm the efficacy of our approach in enhancing image quality across different degradation conditions.

### 4.3 Ablation Studies

We have done several ablation studies to show the contributions and properties of our proposed HAIR.

**Effectiveness of Classifier and Hyper Selecting Net (HSN)** As detailed in Table 4, we study the impact of the proposed modules in four settings: (a) Here, the model aligns with the Restormer architecture [12]. (b) In this configuration, the Global Information Vector (GIV) is directly used as conditional embeddings for the Transformer Blocks in the



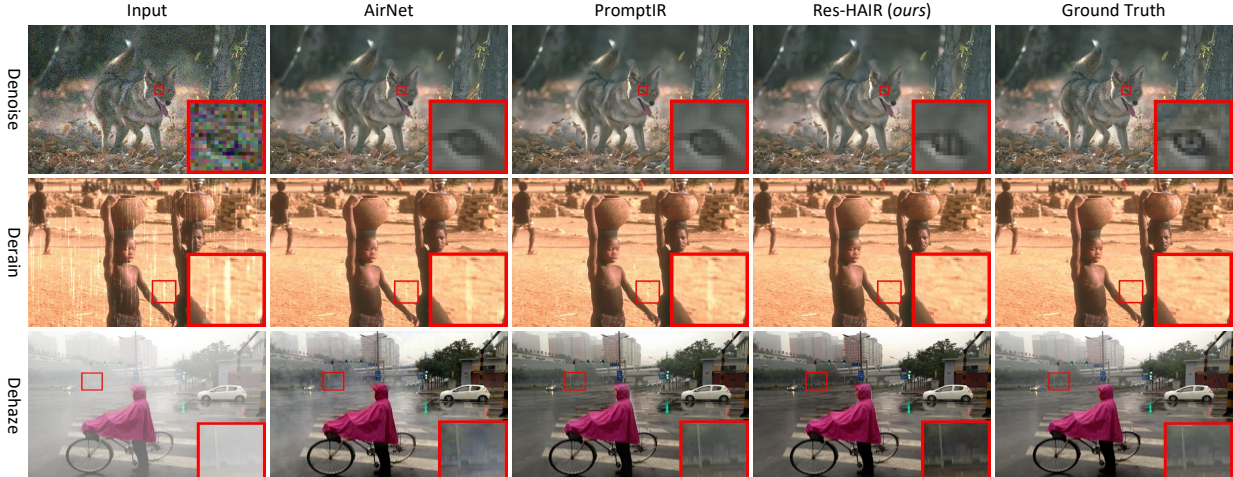


Figure 4: Visual comparison of all-in-one methods in all-in-one degradation settings.

Decoder, rather than for weight generation. (c) The GIVs are designated as independently trainable parameters, each randomly initialized, with the Decoder’s Transformer Blocks having their own distinct GIVs. (d) This setup incorporates both components. The results demonstrate the indispensability of both components. With the addition of only 3M parameters and no change to the logical structure, Res-HAIR outperforms Restormer by 1.7 dB in PSNR, underscoring the simplicity and effectiveness of our proposed approach.

**Position of Classifier (and HyperTrans Blocks)** In our design approach, the Classifier is positioned after the first three Encoder levels, with the subsequent four Decoder levels employing HyperTrans Blocks, constituting a 3+4 configuration. The rationale for this design choice is demonstrated in Table 5. It is evident that the optimal placement for the Classifier is at the network’s midpoint. This positioning takes advantage of the expansive receptive field of the features post the network’s halfway point, while allowing the HSN to dynamically generate parameters for the remaining modules. Furthermore, it is crucial to strike a balance between the receptive field size of the features fed into the Classifier and the count of HyperTrans Blocks utilized, ensuring the model’s efficiency and adaptability.

Table 4: *Impact of key components.* Results are from single deraining task on Rain100L.

Setting	Prams.	Classifier	HSN	PSNR	SSIM
(a) (baseline)	26M	-	-	36.74	.978
(b)	27M	✓	-	36.88	.979
(c)	28M	-	✓	36.76	.979
(d) (ours)	29M	✓	✓	<b>39.00</b>	<b>.985</b>

Table 5: *Impact of position.* Results are from Denoise task on Urban100 ( $\sigma=25$ ).

Setting	(1+6)	(2+5)	(4+3)	(5+2)	(6+1)	(3+4) (ours)
PSNR	32.45	32.56	32.68	32.61	32.51	<b>32.70</b>
SSIM	0.927	0.929	0.931	0.930	0.927	<b>0.931</b>

**HAIR for Other Baselines.** We have previously posited that **HAIR is essentially a plug-in-and-play module** which is readily integrable with any image-to-image network architecture. To substantiate this claim, we have implemented HAIR on various established baselines. As depicted in Table Table 6, we selected three efficacious image restoration models—Transweather [1], AirNet [20], and Restormer [12]—for integration with HAIR. Specifically, we have integrated the Classifier at the network’s midpoint for each method and transitioned the subsequent layers to Hypernetworks-based modules. The outcomes show that our method outperforms PromptIR as a plug-in-and-play module, underscoring the universality and potency of our approach.

## 5 Conclusion

This paper introduces HAIR, a novel plug-and-play Hypernetworks-based module capable of being easily integrated and adaptively generating parameters for different networks based on the input image. Our method comprises two main components: the Classifier and the Hyper Selecting Net (HSN). Specifically, the Classifier is a simple image classification network with Global Average Pooling, designed to produce a Global Information Vector (GIV) that encapsulates the global information from the input image. The HSN functions as a Fully-connected Neural Network,

Table 6: *HAIR for different baselines architectures*. PSNR (dB,  $\uparrow$ ) and SSIM ( $\uparrow$ ) metrics are reported on the full RGB images. **Best** performances are highlighted.

Method	Main Operation	Params	<u>Dehazing</u>		<u>Deraining</u>		<u>Denoising</u>		<u>Deblurring</u>		<u>Low-Light</u>		Average	
			SOTS		Rain100L		BSD68 $_{\sigma=25}$		GoPro		LOLv1			
Transweather [1]		38M	21.32	.885	29.43	.905	29.00	.841	25.12	.757	21.21	.792	25.22	.836
Transweather+PromptIR	Self-Attention	51M	22.89	.920	29.79	.913	29.95	<b>.877</b>	25.74	.781	23.02	.849	26.28	.868
Transweather+HAIR		42M	<b>23.66</b>	<b>.935</b>	<b>32.34</b>	<b>.947</b>	<b>29.96</b>	.875	<b>26.33</b>	<b>.802</b>	<b>23.16</b>	<b>.858</b>	<b>27.09</b>	<b>.884</b>
AirNet [20]		9M	21.04	.884	32.98	.951	30.91	.882	24.35	.781	18.18	.735	25.49	.847
AirNet+PromptIR	Convolution	14M	21.34	.883	33.52	.953	30.92	.882	24.37	.786	18.18	.737	25.67	.848
AirNet+HAIR		10M	<b>22.15</b>	<b>.899</b>	<b>34.56</b>	<b>.957</b>	<b>30.94</b>	<b>.884</b>	<b>25.44</b>	<b>.792</b>	<b>18.24</b>	<b>.740</b>	<b>26.27</b>	<b>.854</b>
Restormer [12]		26M	24.09	.927	34.81	.962	31.49	.884	27.22	.829	20.41	.806	27.60	.881
Restormer+PromptIR	Convolution	36M	30.61	.974	36.17	.973	31.25	.887	27.93	.851	22.89	.842	29.77	.905
Restormer+HAIR		29M	<b>30.62</b>	<b>.978</b>	<b>38.11</b>	<b>.981</b>	<b>31.49</b>	<b>.891</b>	<b>28.52</b>	<b>.874</b>	<b>23.12</b>	<b>.847</b>	<b>30.37</b>	<b>.914</b>

receiving the GIV and outputting parameters for the corresponding modules. Extensive experiments indicate that HAIR can significantly enhance the performance of various image restoration architectures at a low cost without necessitating any changes to their logical structures. By incorporating HAIR into the widely recognized Restormer architecture, we have achieved State-Of-The-Art performance on a range of image restoration tasks. The potential for further exploitation of data-conditioned Hypernetworks in image-to-image tasks is substantial, considering their robust adaptability to diverse input images based on their content.

## References

- [1] Jeya Maria Jose Valanarasu, Rajeev Yasarla, and Vishal M Patel. Transweather: Transformer-based restoration of images degraded by adverse weather conditions. In *Proceedings of the IEEE/CVF Conference on Computer Vision and Pattern Recognition (CVPR)*, 2022.
- [2] Pei Soo-Chang Chen Yu-Wei. Always clear days: Degradation type and severity aware all-in-one adverse weather removal. *arXiv preprint arXiv:2310.18293*, 2023.
- [3] Florin Girbacia, Silviu Butnariu, Alex Petre Orman, and Cristian Cezar Postelnicu. Virtual restoration of deteriorated religious heritage objects using augmented reality technologies. *European Journal of Science and Theology*, 9(2):223–231, 2013.
- [4] Giovanni Saggio, Davide Borra, et al. Augmented reality for restoration/reconstruction of artefacts with artistic or historical value. In *Augmented reality: some emerging application areas*, pages 59–86. InTech Publications, 2011.
- [5] Xin Dang, Hai Wang, Jie Ren, and Le Chen. An application performance optimization model of mobile augmented reality based on hd restoration. In *2020 Eighth International Conference on Advanced Cloud and Big Data (CBD)*, pages 201–206. IEEE, 2020.
- [6] Kai Zhang, Wangmeng Zuo, Shuhang Gu, and Lei Zhang. Learning deep cnn denoiser prior for image restoration. In *Proceedings of the IEEE conference on computer vision and pattern recognition*, pages 3929–3938, 2017.
- [7] Jingyun Liang, Jiezhang Cao, Guolei Sun, Kai Zhang, Luc Van Gool, and Radu Timofte. Swinir: Image restoration using swin transformer. In *Proceedings of the IEEE/CVF international conference on computer vision*, pages 1833–1844, 2021.
- [8] Liangyu Chen, Xiaojie Chu, Xiangyu Zhang, and Jian Sun. Simple baselines for image restoration. In *European conference on computer vision*, pages 17–33. Springer, 2022.
- [9] Ying Tai, Jian Yang, Xiaoming Liu, and Chunyan Xu. Memnet: A persistent memory network for image restoration. In *Proceedings of the IEEE international conference on computer vision*, pages 4539–4547, 2017.
- [10] Jaakko Lehtinen, Jacob Munkberg, Jon Hasselgren, Samuli Laine, Tero Karras, Miika Aittala, and Timo Aila. Noise2noise: Learning image restoration without clean data. *arXiv preprint arXiv:1803.04189*, 2018.
- [11] Yulun Zhang, Kungpeng Li, Kai Li, Bineng Zhong, and Yun Fu. Residual non-local attention networks for image restoration. *arXiv preprint arXiv:1903.10082*, 2019.
- [12] Syed Waqas Zamir, Aditya Arora, Salman Khan, Munawar Hayat, Fahad Shahbaz Khan, and Ming-Hsuan Yang. Restormer: Efficient transformer for high-resolution image restoration. In *Proceedings of the IEEE/CVF conference on computer vision and pattern recognition*, pages 5728–5739, 2022.

- [13] Zheng Chen, Yulun Zhang, Jinjin Gu, Linghe Kong, Xin Yuan, et al. Cross aggregation transformer for image restoration. *Advances in Neural Information Processing Systems*, 35:25478–25490, 2022.
- [14] Zilong Li, Yiming Lei, Chenglong Ma, Junping Zhang, and Hongming Shan. Prompt-in-prompt learning for universal image restoration. *arXiv preprint arXiv:2312.05038*, 2023.
- [15] Akshay Dudhane, Omkar Thawakar, Syed Waqas Zamir, Salman Khan, Fahad Shahbaz Khan, and Ming-Hsuan Yang. Dynamic pre-training: Towards efficient and scalable all-in-one image restoration. 2024.
- [16] Yulun Zhang, Yapeng Tian, Yu Kong, Bineng Zhong, and Yun Fu. Residual dense network for image super-resolution. In *Proceedings of the IEEE Conference on Computer Vision and Pattern Recognition*, 2018.
- [17] Syed Waqas Zamir, Aditya Arora, Salman Khan, Munawar Hayat, Fahad Shahbaz Khan, Ming-Hsuan Yang, and Ling Shao. Cycleisp: Real image restoration via improved data synthesis. In *Proceedings of the IEEE/CVF conference on computer vision and pattern recognition*, pages 2696–2705, 2020.
- [18] Syed Waqas Zamir, Aditya Arora, Salman Khan, Munawar Hayat, Fahad Shahbaz Khan, Ming-Hsuan Yang, and Ling Shao. Learning enriched features for real image restoration and enhancement. In *Computer Vision–ECCV 2020: 16th European Conference, Glasgow, UK, August 23–28, 2020, Proceedings, Part XXV 16*, pages 492–511. Springer, 2020.
- [19] Kuldeep Purohit, Maitreya Suin, AN Rajagopalan, and Vishnu Naresh Boddeti. Spatially-adaptive image restoration using distortion-guided networks. In *Proceedings of the IEEE/CVF international conference on computer vision*, pages 2309–2319, 2021.
- [20] Boyun Li, Xiao Liu, Peng Hu, Zhongqin Wu, Jiancheng Lv, and Xi Peng. All-in-one image restoration for unknown corruption. In *Proceedings of the IEEE/CVF conference on computer vision and pattern recognition*, pages 17452–17462, 2022.
- [21] Syed Waqas Zamir, Aditya Arora, Salman Khan, Munawar Hayat, Fahad Shahbaz Khan, Ming-Hsuan Yang, and Ling Shao. Multi-stage progressive image restoration. In *Proceedings of the IEEE/CVF Conference on Computer Vision and Pattern Recognition (CVPR)*, 2021.
- [22] Lin Liu, Lingxi Xie, Xiaopeng Zhang, Shanxin Yuan, Xiangyu Chen, Wengang Zhou, Houqiang Li, and Qi Tian. Tape: Task-agnostic prior embedding for image restoration. In *Proceedings of the European Conference on Computer Vision (ECCV)*, 2022.
- [23] Qingnan Fan, Dongdong Chen, Lu Yuan, Gang Hua, Nenghai Yu, and Baoquan Chen. A general decoupled learning framework for parameterized image operators. *IEEE transactions on pattern analysis and machine intelligence*, 43(1):33–47, 2019.
- [24] Vaishnav Potlapalli, Syed Waqas Zamir, Salman H Khan, and Fahad Shahbaz Khan. Promptir: Prompting for all-in-one image restoration. *Advances in Neural Information Processing Systems*, 36, 2024.
- [25] Jinghao Zhang, Jie Huang, Mingde Yao, Zizheng Yang, Hu Yu, Man Zhou, and Feng Zhao. Ingredient-oriented multi-degradation learning for image restoration. In *Proceedings of the IEEE/CVF Conference on Computer Vision and Pattern Recognition*, pages 5825–5835, 2023.
- [26] Eduard Zamfir, Zongwei Wu, Nancy Mehta, Danda Dani Paudel, Yulun Zhang, and Radu Timofte. Efficient degradation-aware any image restoration. *arXiv preprint arXiv:2405.15475*, 2024.
- [27] Cong Wang, Jinshan Pan, Wei Wang, Jiangxin Dong, Mengzhu Wang, Yakun Ju, and Junyang Chen. Promptrestorer: A prompting image restoration method with degradation perception. *Advances in Neural Information Processing Systems*, 36:8898–8912, 2023.
- [28] Akshay Dudhane, Omkar Thawakar, Syed Waqas Zamir, Salman Khan, Ming-Hsuan Yang, and Fahad Shahbaz Khan. Dynamic pre-training: Towards efficient and scalable all-in-one image restoration, 2024.
- [29] David Ha, Andrew Dai, and Quoc V. Le. Hypernetworks, 2016.
- [30] Yitong Jiang, Zhaoyang Zhang, Tianfan Xue, and Jinwei Gu. Autodir: Automatic all-in-one image restoration with latent diffusion. *arXiv preprint arXiv:2310.10123*, 2023.
- [31] Wayne Xin Zhao, Kun Zhou, Junyi Li, Tianyi Tang, Xiaolei Wang, Yupeng Hou, Yingqian Min, Beichen Zhang, Junjie Zhang, Zican Dong, et al. A survey of large language models. *arXiv preprint arXiv:2303.18223*, 2023.
- [32] Tomer Galanti and Lior Wolf. On the modularity of hypernetworks. *Advances in Neural Information Processing Systems*, 33:10409–10419, 2020.
- [33] D. Lu and Q. Weng. A survey of image classification methods and techniques for improving classification performance. *International Journal of Remote Sensing*, 28(5):823–870, 2007.

- [34] Dengsheng Lu and Qihao Weng. A survey of image classification methods and techniques for improving classification performance. *International journal of Remote sensing*, 28(5):823–870, 2007.
- [35] Kaiming He, Xiangyu Zhang, Shaoqing Ren, and Jian Sun. Deep residual learning for image recognition. In *Proceedings of the IEEE conference on computer vision and pattern recognition*, pages 770–778, 2016.
- [36] Alexey Dosovitskiy, Lucas Beyer, Alexander Kolesnikov, Dirk Weissenborn, Xiaohua Zhai, Thomas Unterthiner, Mostafa Dehghani, Matthias Minderer, Georg Heigold, Sylvain Gelly, et al. An image is worth 16x16 words: Transformers for image recognition at scale. *arXiv preprint arXiv:2010.11929*, 2020.
- [37] Ze Liu, Yutong Lin, Yue Cao, Han Hu, Yixuan Wei, Zheng Zhang, Stephen Lin, and Baining Guo. Swin transformer: Hierarchical vision transformer using shifted windows. In *Proceedings of the IEEE/CVF international conference on computer vision*, pages 10012–10022, 2021.
- [38] Lianghai Zhu, Bencheng Liao, Qian Zhang, Xinlong Wang, Wenyu Liu, and Xinggang Wang. Vision mamba: Efficient visual representation learning with bidirectional state space model. *arXiv preprint arXiv:2401.09417*, 2024.
- [39] Jia Deng, Wei Dong, Richard Socher, Li-Jia Li, Kai Li, and Li Fei-Fei. Imagenet: A large-scale hierarchical image database. In *2009 IEEE conference on computer vision and pattern recognition*, pages 248–255. Ieee, 2009.
- [40] Vinod Kumar Chauhan, Jiandong Zhou, Ping Lu, Soheila Molaei, and David A Clifton. A brief review of hypernetworks in deep learning. *arXiv preprint arXiv:2306.06955*, 2023.
- [41] Yuval Nirkin, Lior Wolf, and Tal Hassner. Hyperseg: Patch-wise hypernetwork for real-time semantic segmentation. In *Proceedings of the IEEE/CVF conference on computer vision and pattern recognition*, pages 4061–4070, 2021.
- [42] Yuval Alaluf, Omer Tov, Ron Mokady, Rinon Gal, and Amit Bermano. Hyperstyle: Stylegan inversion with hypernetworks for real image editing. In *Proceedings of the IEEE/CVF conference on computer Vision and pattern recognition*, pages 18511–18521, 2022.
- [43] Shai Aharon and Gil Ben-Artzi. Hypernetwork-based adaptive image restoration. In *ICASSP 2023-2023 IEEE International Conference on Acoustics, Speech and Signal Processing (ICASSP)*, pages 1–5. IEEE, 2023.
- [44] Karen Simonyan and Andrew Zisserman. Very deep convolutional networks for large-scale image recognition. *arXiv preprint arXiv:1409.1556*, 2014.
- [45] Christian Szegedy, Vincent Vanhoucke, Sergey Ioffe, Jon Shlens, and Zbigniew Wojna. Rethinking the inception architecture for computer vision. In *Proceedings of the IEEE conference on computer vision and pattern recognition*, pages 2818–2826, 2016.
- [46] Ashish Vaswani, Noam Shazeer, Niki Parmar, Jakob Uszkoreit, Llion Jones, Aidan N Gomez, Łukasz Kaiser, and Illia Polosukhin. Attention is all you need. *Advances in neural information processing systems*, 30, 2017.
- [47] Albert Gu and Tri Dao. Mamba: Linear-time sequence modeling with selective state spaces. *arXiv preprint arXiv:2312.00752*, 2023.
- [48] Ilya Loshchilov, Frank Hutter, et al. Fixing weight decay regularization in adam. *arXiv preprint arXiv:1711.05101*, 5, 2017.
- [49] Pablo Arbelaez, Michael Maire, Charless Fowlkes, and Jitendra Malik. Contour detection and hierarchical image segmentation. *IEEE transactions on pattern analysis and machine intelligence*, 33(5):898–916, 2010.
- [50] Kede Ma, Zhengfang Duanmu, Qingbo Wu, Zhou Wang, Hongwei Yong, Hongliang Li, and Lei Zhang. Waterloo exploration database: New challenges for image quality assessment models. *IEEE Transactions on Image Processing*, 26(2):1004–1016, 2016.
- [51] David Martin, Charless Fowlkes, Doron Tal, and Jitendra Malik. A database of human segmented natural images and its application to evaluating segmentation algorithms and measuring ecological statistics. In *ICCV*, 2001.
- [52] Jia-Bin Huang, Abhishek Singh, and Narendra Ahuja. Single image super-resolution from transformed self-exemplars. In *Proceedings of the IEEE conference on computer vision and pattern recognition*, pages 5197–5206, 2015.
- [53] Fuzhi Yang, Huan Yang, Jianlong Fu, Hongtao Lu, and Baining Guo. Learning texture transformer network for image super-resolution. In *CVPR*, 2020.
- [54] Boyi Li, Wenqi Ren, Dengpan Fu, Dacheng Tao, Dan Feng, Wenjun Zeng, and Zhangyang Wang. Benchmarking single-image dehazing and beyond. *IEEE Transactions on Image Processing*, 28(1):492–505, 2018.
- [55] Seungjun Nah, Tae Hyun Kim, and Kyoung Mu Lee. Deep multi-scale convolutional neural network for dynamic scene deblurring. In *Proceedings of the IEEE conference on computer vision and pattern recognition*, pages 3883–3891, 2017.

- [56] Chen Wei, Wenjing Wang, Wenhan Yang, and Jiaying Liu. Deep retinex decomposition for low-light enhancement. *arXiv preprint arXiv:1808.04560*, 2018.
- [57] Chunwei Tian, Yong Xu, and Wangmeng Zuo. Image denoising using deep cnn with batch renormalization. *Neural Networks*, 2020.
- [58] Hongyun Gao, Xin Tao, Xiaoyong Shen, and Jiaya Jia. Dynamic scene deblurring with parameter selective sharing and nested skip connections. In *Proceedings of the IEEE/CVF Conference on Computer Vision and Pattern Recognition (CVPR)*, 2019.
- [59] Yu Dong, Yihao Liu, He Zhang, Shifeng Chen, and Yu Qiao. Fd-gan: Generative adversarial networks with fusion-discriminator for single image dehazing. In *Proceedings of the AAAI conference on artificial intelligence (AAAI)*, 2020.
- [60] Chong Mou, Qian Wang, and Jian Zhang. Deep generalized unfolding networks for image restoration. In *Proceedings of the IEEE/CVF Conference on Computer Vision and Pattern Recognition*, pages 17399–17410, 2022.
- [61] Bolun Cai, Xiangmin Xu, Kui Jia, Chunmei Qing, and Dacheng Tao. Dehazenet: An end-to-end system for single image haze removal. *IEEE Transactions on Image Processing*, 25(11):5187–5198, 2016.
- [62] Wenqi Ren, Si Liu, Hua Zhang, Jinshan Pan, Xiaochun Cao, and Ming-Hsuan Yang. Single image dehazing via multi-scale convolutional neural networks. In *Computer Vision–ECCV 2016: 14th European Conference, Amsterdam, The Netherlands, October 11–14, 2016, Proceedings, Part II 14*, pages 154–169. Springer, 2016.
- [63] Yanyun Qu, Yizi Chen, Jingying Huang, and Yuan Xie. Enhanced pix2pix dehazing network. In *CVPR*, pages 8160–8168, 2019.
- [64] He Zhang and Vishal M Patel. Density-aware single image de-raining using a multi-stream dense network. In *CVPR*, 2018.
- [65] Rajeev Yasarla and Vishal M Patel. Uncertainty guided multi-scale residual learning-using a cycle spinning cnn for single image de-raining. In *CVPR*, 2019.
- [66] Wei Wei, Deyu Meng, Qian Zhao, Zongben Xu, and Ying Wu. Semi-supervised transfer learning for image rain removal. In *CVPR*, 2019.
- [67] Kui Jiang, Zhongyuan Wang, Peng Yi, Chen Chen, Baojin Huang, Yimin Luo, Jiayi Ma, and Junjun Jiang. Multi-scale progressive fusion network for single image deraining. In *CVPR*, pages 8346–8355, 2020.
- [68] Kostadin Dabov, Alessandro Foi, Vladimir Katkovnik, and Karen Egiazarian. Color image denoising via sparse 3d collaborative filtering with grouping constraint in luminance-chrominance space. In *2007 IEEE International Conference on Image Processing*, volume 1, pages I–313. IEEE, 2007.
- [69] Kai Zhang, Wangmeng Zuo, Yunjin Chen, Deyu Meng, and Lei Zhang. Beyond a gaussian denoiser: Residual learning of deep cnn for image denoising. *IEEE transactions on image processing*, 26(7):3142–3155, 2017.
- [70] Kai Zhang, Wangmeng Zuo, and Lei Zhang. Ffdnet: Toward a fast and flexible solution for cnn-based image denoising. *IEEE Transactions on Image Processing*, 27(9):4608–4622, 2018.

## 6 Appendix

### 6.1 Detailed Proof of Theorem 1, Theorem 2

**Notations** We consider  $\mathcal{X} = [-1, 1]^{m_1}$  and  $\mathcal{I} = [-1, 1]^{m_2}$  and denote,  $m := m_1 + m_2$ . Here  $\mathcal{X}$  stands for the set of input images  $\mathbf{X}$ , meanwhile  $\mathcal{I}$  refers to the set of degradation information  $e(\mathbf{X})$ . For a closed set  $X \subset \mathbb{R}^n$ , we denote by  $C^r(X)$  the linear space of all  $r$ -continuously differentiable functions  $h : X \rightarrow \mathbb{R}$  on  $X$  equipped with the supremum norm  $\|h\|_\infty := \max_{x \in X} \|h(x)\|_1$ .

**Theorem 3.** (The **Theorem 2** in [32]) Let  $\sigma$  be a universal, piece-wise  $C^1(\mathbb{R})$  activation function with  $\sigma' \in BV(\mathbb{R})$  and  $\sigma(0) = 0$ . Let  $\mathcal{E}_{\mathbf{e}, \mathbf{q}}$  be a neural embedding method. Assume that  $\mathbf{e}$  is a class of continuously differentiable neural network  $e$  with zero biases, output dimension  $k = \mathcal{O}(1)$  and  $\mathcal{C}(e) \leq \ell_1$  and  $\mathbf{q}$  is a class of neural networks  $q$  with  $\sigma$  activations and  $\mathcal{C}(q) \leq \ell_2$ . Let  $\mathbb{Y} := \mathcal{W}_{1, m}$ . Assume that any non-constant  $y \in \mathbb{Y}$  cannot be represented as a neural network with  $\sigma$  activations. If the embedding method achieves error  $d(\mathcal{E}_{\mathbf{e}, \mathbf{q}}, \mathbb{Y}) \leq \epsilon$ , then, the complexity of  $\mathbf{q}$  is:  $N_{\mathbf{q}} = \Omega(\epsilon^{-(m_1 + m_2)})$ .

The notation  $BV(\mathbb{R})$  stands for the set of functions of bounded variation,

$$BV(\mathbb{R}) := \{f \in L^1(\mathbb{R}) \mid \|f\|_{BV} < \infty\} \text{ where, } \|f\|_{BV} := \sup_{\substack{\phi \in C_c^1(\mathbb{R}) \\ \|\phi\|_\infty \leq 1}} \int_{\mathbb{R}} f(x) \cdot \phi(x) \, dx \quad (10)$$

Note that a distinct neural network  $e$  is not mandatory. For example, the "prompts" in PromptIR [24] are a set of trainable parameters that do not require a separate network to generate them. Yet, the conclusion remains the same even if network  $e$  is non-existent.

**Theorem 4.** (The **Theorem 3** in [32]) *In the setting of Theorem 3, except  $k$  is not necessarily  $\mathcal{O}(1)$ . Assume that the first layer of any  $q \in \mathbf{q}$  is bounded  $\|W^1\|_1 \leq c$ , for some constant  $c > 0$ . If the embedding method achieves error  $d(\mathcal{E}_{e,\mathbf{q}}, \mathbb{Y}) \leq \epsilon$ , then, the complexity of  $\mathbf{q}$  is:  $N_{\mathbf{q}} = \Omega(\epsilon^{-\min(m, 2m_1)})$ .*

**Theorem 5.** (The **Theorem 4** in [32]) *Let  $\sigma$  be as in Theorem 3. Let  $y \in \mathbb{Y} = \mathcal{W}_{r,m}$  be a function, such that,  $y_I$  cannot be represented as a neural network with  $\sigma$  activations for all  $I \in \mathcal{I}$ . Then, there is a class,  $\mathbf{g}$ , of neural networks with  $\sigma$  activations and a network  $f(I; \theta_f)$  with ReLU activations, such that,  $h(x, I) = g(x; f(I; \theta_f))$  achieves error  $\leq \epsilon$  in approximating  $y$  and  $N_{\mathbf{g}} = \mathcal{O}(\epsilon^{-m_1/r})$ .*

In the realm of image restoration,  $m_1$  equals  $3HW$ , and  $m_2$  equals  $k$ , where  $k$  denotes the dimensionality of the flattened degradation embedding. In our method,  $k$  is consistent with the shape of the Global Information Vector (GIV), specifically  $2C$ , and thus is  $\mathcal{O}(1)$ . Conversely, in PromptIR [24],  $k$  is dynamic and contingent on the resolution of the input image, precluding it from being  $\mathcal{O}(1)$ . Theorem 5 indicates that the complexity for a Hypernetworks-based method to attain an error of  $\epsilon$  is  $\mathcal{O}(\epsilon^{-3HW/r})$ . Theorems 3 and 4 collectively suggest that the complexity for embedding-based methods is at least  $\Omega(\epsilon^{-\min(3HW+k, 6HW)})$ . This comparison illustrates that Hypernetworks-based methods like HAIR may require fewer parameters to reach a given error threshold compared to their embedding-based counterparts.

## 6.2 Visual Results

In Fig. 5, Fig. 6 we provide more visual results to show the strong ability of our method for image restoration tasks.

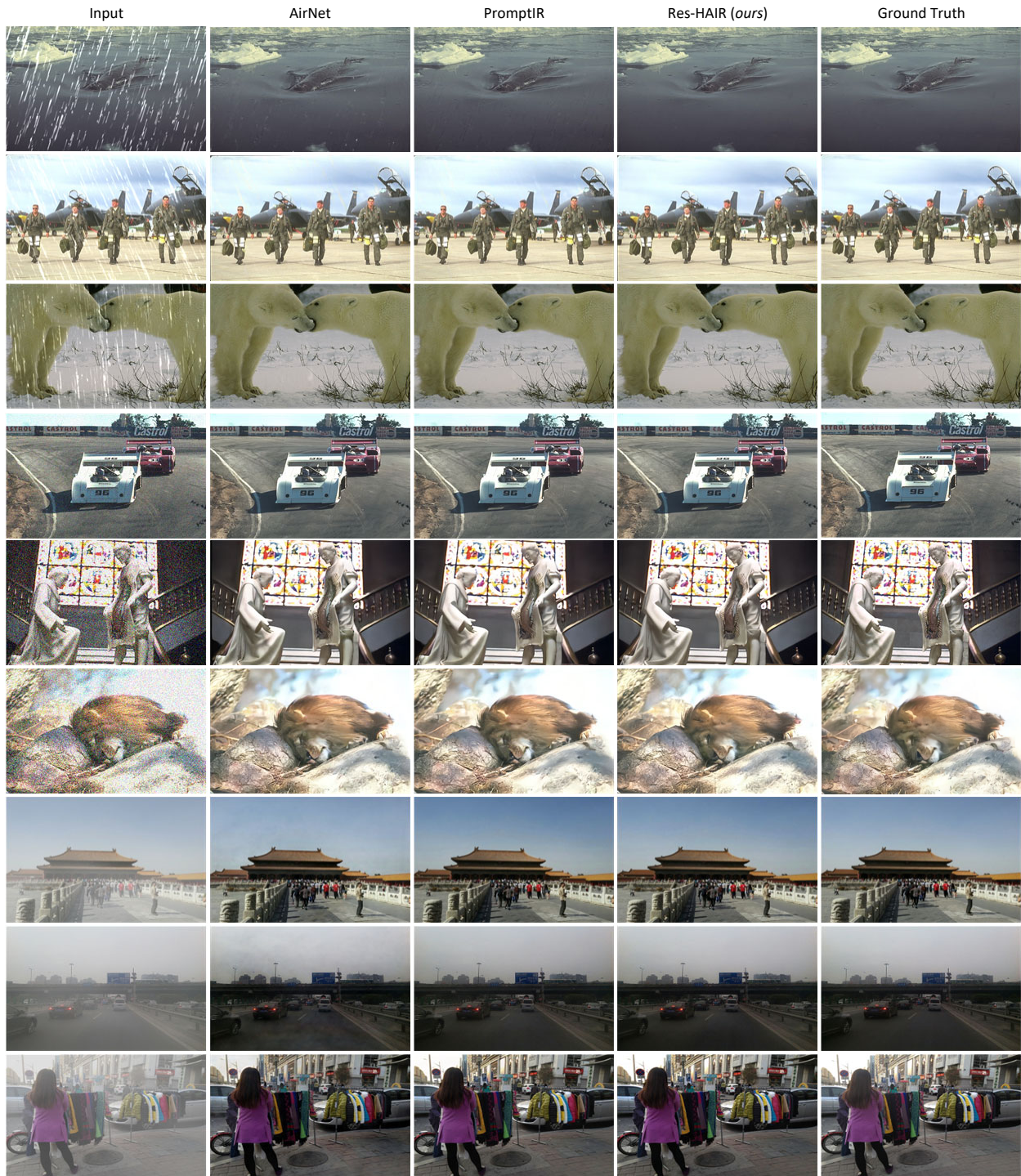


Figure 5: Additional visual results.

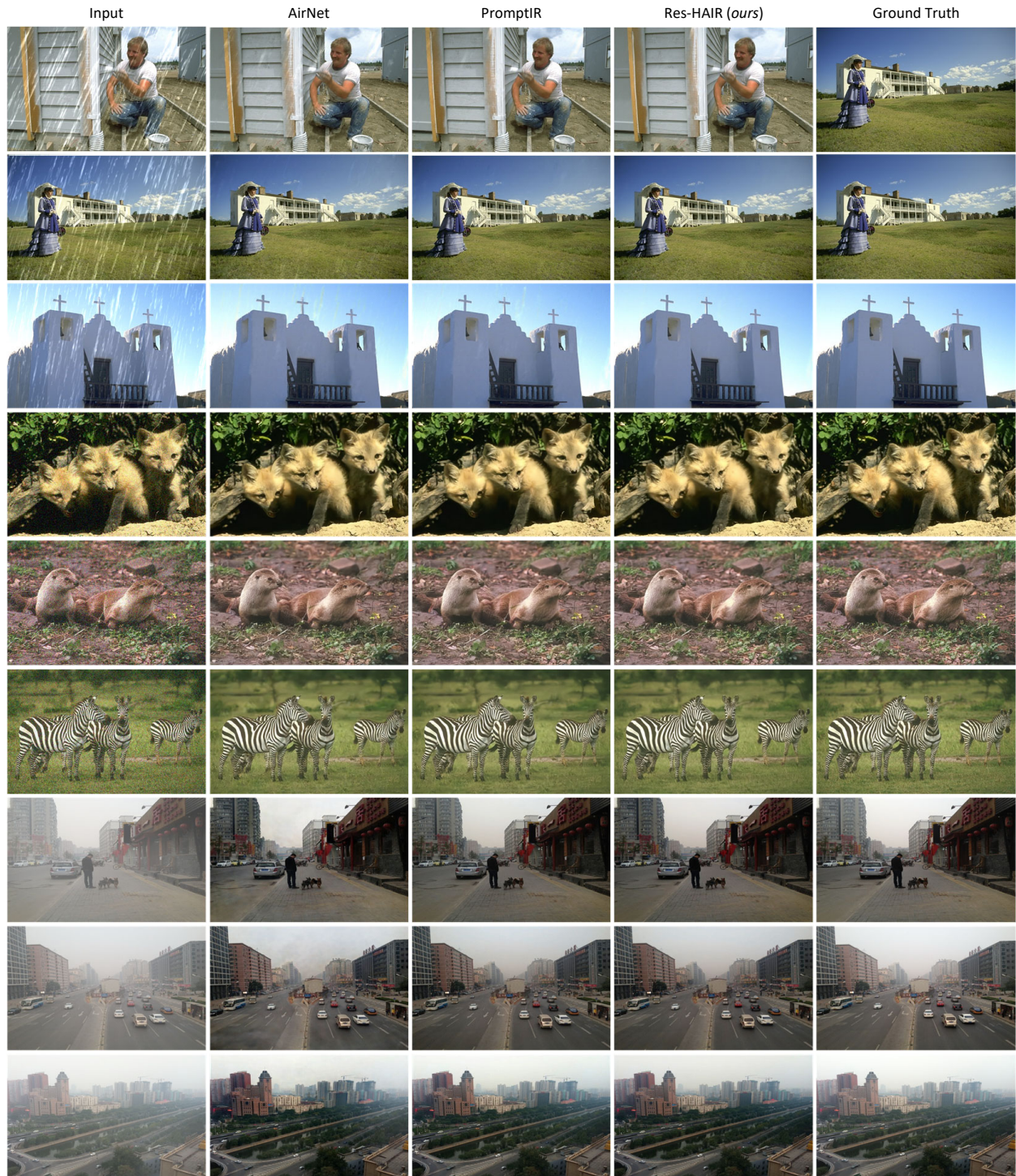


Figure 6: Additional visual results